

## METALLIC LINE PROFILES OF THE A0 V STAR VEGA

AUSTIN F. GULLIVER<sup>1</sup>

Department of Physics and Astronomy, Brandon University, Brandon, Manitoba, Canada R7A 6A9

SAUL J. ADELMAN<sup>1</sup>

Department of Physics, The Citadel, Charleston, SC 29409

CHARLES R. COWLEY<sup>1</sup>

Department of Astronomy, University of Michigan, Ann Arbor, MI 48109

AND

J. MURRAY FLETCHER

Dominion Astrophysical Observatory, 5071 West Saanich Road, R.R.5, Victoria, BC, Canada V8X 4M6

Received 1990 August 24; accepted 1991 April 24

### ABSTRACT

High-dispersion ( $2.4 \text{ \AA mm}^{-1}$ ) ultrahigh signal-to-noise ratio Reticon spectra of Vega have been obtained with the coudé spectrograph of the 1.2 m telescope of the Dominion Astrophysical Observatory. A mean signal-to-noise ratio of 2500 over the spectral region  $\lambda\lambda 3825\text{--}5435$  has been achieved. Examination of the line profiles has confirmed the presence of two distinct types of profiles which had been previously seen in IIIa-J and lower signal-to-noise ratio Reticon spectra. The profiles of the strong lines are essentially classical rotational profiles with enhanced wings. The weak lines are clearly flat-bottomed resulting in a trapezoidal appearance. Vega is not unique in this respect as 10 Tri,  $\nu$  Cap,  $\beta$  PsA, and possibly several other stars with spectral types near A0, have similar line profiles. A few possible theoretical explanations are presented. For example, these profiles might be the result of a rapidly rotating star seen nearly pole-on.

*Subject headings:* line profiles — stars: individual ( $\alpha$  Lyrae) — stars: rotation

### 1. INTRODUCTION

Vega ( $\alpha$  Lyr = HR 7001 = HD 172167) is the primary photometric standard. It is very bright and relatively sharp-lined and has been studied extensively. Its photospheric abundances show it is metal-weak, but these chemical anomalies are sufficiently mild that only recently has it been possible to demonstrate their extent definitively (see Adelman & Gulliver 1990; Gigas 1986; Sadakane, Nishimura, & Hirata 1986). In 1971 JMF attempted to monitor the radial velocity of Vega for periodic variations. He used the 9682M camera of the 1.2 m telescope coudé spectrograph of the Dominion Astrophysical Observatory with a reciprocal dispersion of  $2.4 \text{ \AA mm}^{-1}$  and IIIa-J photographic emulsions. While measuring these plates on a scanning oscilloscope-display measuring machine, JMF noted that some of the weakest lines appeared to have flat bottoms. The first spectrogram which showed such line profiles was plate 7108, dated 1971 September 1. Since the spectrograph and photographic plate combination did not have sufficient signal-to-noise ratio, further investigation of the flat-bottomed profiles was postponed.

### 2. OBSERVATIONAL DATA

A decade and a half later, C. R. C. observed Vega using a  $1 \times 1872$  bare Reticon with  $15 \mu\text{m}$  pixels and the same telescope-camera combination (see Adelman & Gulliver 1990). The instrumental profile of the spectrograph plus Reticon has a FWHM of  $0.074 \text{ \AA}$  (Gulliver & Hill 1990; Booth, Blackwell, & Fletcher 1990). In the last two years, A. F. G. and S. J. A. have obtained still higher signal-to-noise ratio ( $>2000$ ) Reticon data. J. M. F. asked the other coauthors whether they

too had found flat-bottomed lines and kept reminding them about how unusual they were.

We tried various techniques to achieve as high a signal-to-noise ratio as possible: co-adding of both multiple lamps and multiple spectra, bracketing spectra with lamp exposures, use of different lamp illuminations including a broad-lined star, varying of lamp exposure lengths, use of high- and low-gain settings on the Reticon amplifiers, and assiduous cleaning of the Reticon window. The strategy that gives the best results includes (1) a stop designed to reproduce the secondary mirror shadow is placed in the beam (this is especially important for the lamp exposure), (2) the use of the low-gain setting to acquire more photons, (3) the integration of exposures to about 10,000 ADC counts, (4) the use of only a single lamp exposure taken just before the stellar exposure, and finally, (5) taking either one or a pair of stellar exposures bracketed by comparison spectra. A further important development is the modification of the RET72 and PLOTFITS routines (Hill & Fisher 1986) to allow immediate reduction and monitoring of the spectra at the telescope to ascertain their quality. Despite careful controls, on-line reduction is a necessity given the inevitable vagaries of the Reticon at this ultrahigh signal-to-noise ratio.

Initial reductions use the program RET72 (Hill & Fisher 1986) which allows for division by the lamps, normalization of amplifier gains, and FITS file output. A correction for cross talk between channels (Walker et al. 1990) is important for any strong absorption or emission lines. The program REDUCE (Hill & Fisher 1986) measures the comparison spectra and reproduces the stellar spectra in wavelength steps of  $0.035 \text{ \AA}$ . A 4% correction for scattered light (J. M. Fletcher, private communication) is applied for the purposes of this investigation. During the rectification step, a mean signal-to-noise ratio

<sup>1</sup> Visiting Observer, Dominion Astrophysical Observatory.

is determined from the continuum points themselves. The mean value for all 29 sections covering the  $\lambda\lambda 3825\text{--}5435$  region is about 2500.

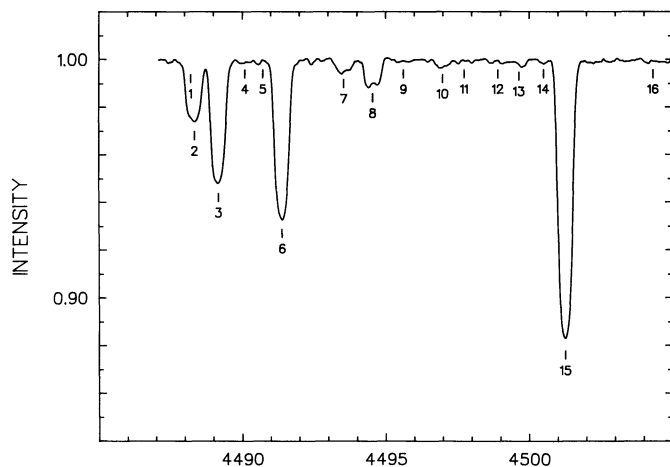
### 3. THE LINE PROFILES

Figure 1 shows a sample spectrum of Vega centered at  $\lambda 4520$ . This section results from the co-addition of two exposures and has a mean signal-to-noise ratio of some 3200. Also shown in Figure 1 are the line centers determined by measuring the spectrum using the program VLINE (Hill & Fisher 1986) and labeled with reference to Table 1. The continuum has been rectified to unity.

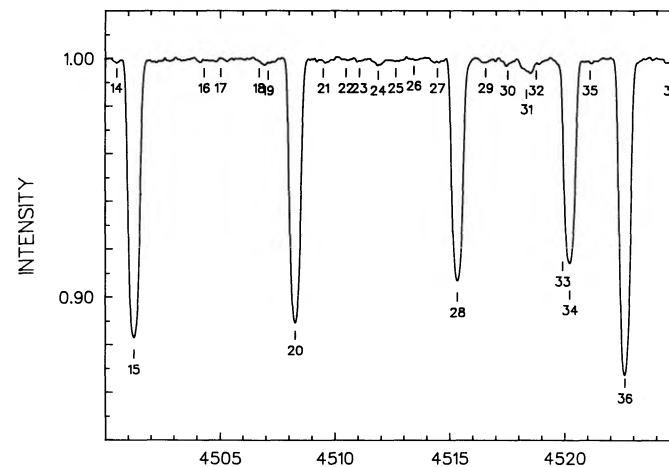
We have used a modified version of VLINESUM (Hill & Fisher 1986) to create two "standard profiles" for use in wavelength and equivalent width measurements. These profiles are preferred to the Gaussian or Voigt profiles often used for these purposes. The general fitting procedure is described by Hill and Fisher.

The success achieved using the two standard profiles can be judged from Figure 2 which is an enlarged view of the profiles fitted to 14 features in the region  $\lambda\lambda 4538\text{--}4549$ . To obtain the optimum fit to the observed spectrum, the weak lines are fitted with a standard profile with a fixed  $v \sin i$  of  $20.2 \text{ km s}^{-1}$ , the value determined from the stronger lines. All other parameters of the fit are allowed to vary. The data for each line including its measured wavelength, equivalent width, central depth, FWHM, and  $v \sin i$  are shown in Table 1. The tentative identifications include results from the routines LINEID and IDPROC (Gulliver & Stadel 1990) as well as the synthetic spectrum of Kurucz (1991) (shown as multiplet KZ). To produce consistent line identifications, all available Reticon and photographic line data from  $\lambda\lambda 3600\text{--}4920$  have also been considered by these routines.

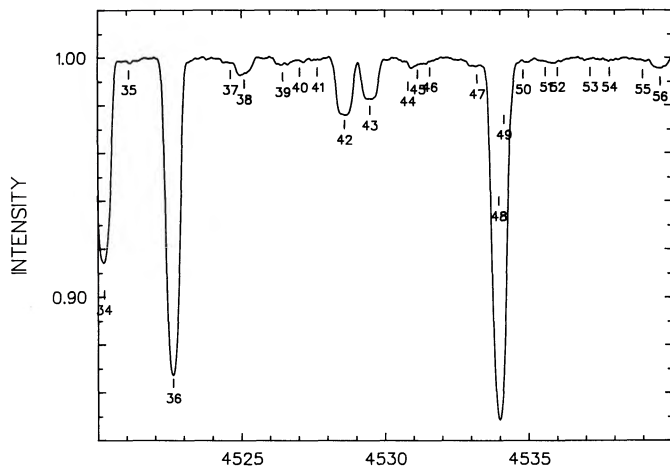
The shapes of weak and strong lines are sufficiently distinct that two standard profiles are required. The strong-line standard profile is essentially a classical rotational profile (cf. Unsöld 1955, eq. [123.11]) with enhanced wings.



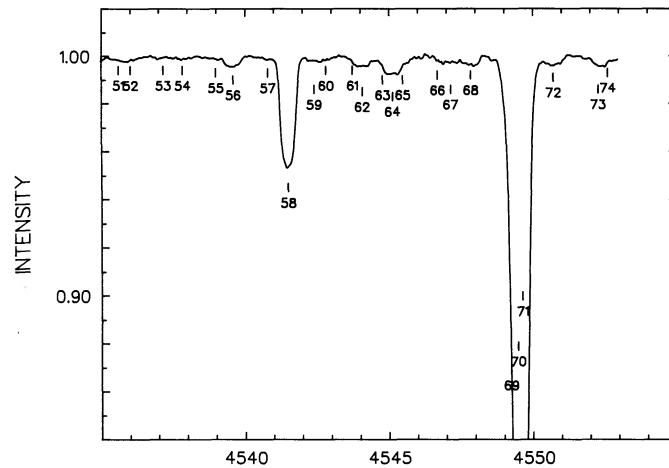
WAVELENGTH  
FIG. 1a



WAVELENGTH  
FIG. 1b



WAVELENGTH  
FIG. 1c



WAVELENGTH  
FIG. 1d

FIG. 1.—(a) Spectrum of Vega with spectral line data referenced in Table 1. (b) Same as (a). (c) Same as (a). (d) Same as (a).

TABLE 1  
SPECTRAL LINE DATA

<i>N</i>	$\lambda$ (Å)	EW (mÅ)	Depth	FWHM (Å)	$V \sin i$ (km s <sup>-1</sup> )	Identification
1.....	4488.202	1.5	0.003	0.61	20.2f	Fe I (819) 4488.140
2.....	4488.337	13.4	0.022	0.61	20.2f	Ti II (115) 4488.319
3.....	4489.173	28.4	0.053	0.55	18.3	Fe II (37) 4489.185
4.....	4490.099	0.7	0.001	0.61	20.2f	Fe I (469) 4490.084
5.....	4490.727	0.7	0.001	0.61	20.2f	Fe I (974) 4490.773 Fe I (973) 4490.773
6.....	4491.397	35.7	0.068	0.54	18.0	Fe II (37) 4491.401
7.....	4493.548	3.0	0.005	0.61	20.2f	Ti II (18) 4493.530
8.....	4494.553	6.7	0.011	0.61	20.2f	Fe I (68) 4494.568
9.....	4495.621	0.5	0.001	0.61	20.2f	Fe II (147) 4495.520 Fe I (827) 4495.566
10.....	4496.992	1.7	0.003	0.61	20.2f	Zr II (40) 4496.960
11.....	4497.739	0.6	0.001	0.61	20.2f	[Na I (15) 4497.657]
12.....	4498.909	0.8	0.001	0.61	20.2f	Mn I (22) 4498.897
13.....	4499.641	1.3	0.002	0.61	20.2f	Fe II (KZ) 4499.688
14.....	4500.498	0.5	0.001	0.33	11.0	[Mn II (KZ) 4500.543]
15.....	4501.269	63.5	0.118	0.55	18.2	Ti II (31) 4501.270
16.....	4504.317	0.7	0.001	0.61	20.2f	Fe II (KZ) 4504.343
17.....	4505.036	0.5	0.001	0.61	20.2f	Ca I (24) 4505.000
18.....	4506.708	0.5	0.001	0.61	20.2f	Ti II (30) 4506.740
19.....	4507.098	1.1	0.002	0.61	20.2f	Fe II (KZ) 4507.102
20.....	4508.280	57.2	0.110	0.53	17.6	Fe II (38) 4508.283
21.....	4509.491	0.7	0.001	0.61	20.2f	Ca I (24) 4509.446
22.....	4510.479	0.2	0.001	0.43	14.3	Fe II (KZ) 4510.513
23.....	4511.060	0.3	0.001	0.34	11.2	Fe I (970) 4511.040
24.....	4511.876	1.3	0.002	0.61	20.2f	Cr II (191) 4511.820 Cr I (150) 4511.903 Ti I (42) 4512.734
25.....	4512.637	0.6	0.001	0.61	20.2f	Unidentified line
26.....	4513.429	0.2	0.000	0.61	20.2f	Unidentified line
27.....	4514.454	0.8	0.001	0.61	20.2f	Cr I (KZ) 4514.459
28.....	4515.337	49.2	0.093	0.54	17.9	Fe II (37) 4515.337
29.....	4516.551	0.8	0.001	0.61	20.2f	Cr II (191) 4516.560
30.....	4517.510	1.2	0.002	0.61	20.2f	Fe I (472) 4517.530
31.....	4518.326	2.9	0.005	0.61	20.2f	Ti II (18) 4518.300
32.....	4518.747	1.2	0.002	0.61	20.2f	Ti I (112) 4518.700
33.....	4519.908	1.5	0.002	0.61	20.2f	Ni I (51) 4519.986
34.....	4520.220	44.8	0.085	0.54	17.9	Fe II (37) 4520.225
35.....	4521.098	0.9	0.002	0.61	20.2f	Cr I (287) 4521.141
36.....	4522.627	69.0	0.131	0.53	17.7	Fe II (38) 4522.634
37.....	4524.636	1.0	0.002	0.61	20.2f	Ti II (60) 4524.732
38.....	4525.115	3.7	0.006	0.61	20.2f	Fe I (826) 4525.142
39.....	4526.461	1.6	0.003	0.61	20.2f	Cr I (33) 4526.466
40.....	4527.053	0.7	0.001	0.61	20.2f	Ca I (36) 4526.935
41.....	4527.666	0.4	0.001	0.61	20.2f	[Fe I (641) 4527.796]
42.....	4528.606	14.6	0.024	0.62	20.4	Fe I (68) 4528.619
43.....	4529.487	10.6	0.017	0.62	20.5	Ti II (82) 4529.465
44.....	4530.809	1.1	0.002	0.61	20.2f	Cr I (33) 4530.755
45.....	4531.151	1.4	0.002	0.61	20.2f	Fe I (39) 4531.152
46.....	4531.579	0.6	0.001	0.61	20.2f	Fe I (555) 4531.633 Fe I (847) 4531.633 Fe I (992) 4531.633 Ti I (42) 4533.238
47.....	4533.218	2.2	0.004	0.61	20.2f	Ti I (42) 4533.238
48.....	4533.959	69.8	0.129	0.55	18.2	Ti II (50) 4533.966
49.....	4534.151	14.5	0.024	0.61	20.2f	Fe II (37) 4534.166
50.....	4534.821	1.0	0.002	0.61	20.2f	Ti I (42) 4534.782
51.....	4535.600	0.9	0.001	0.61	20.2f	Ti I (42) 4535.574
52.....	4536.023	0.9	0.001	0.61	20.2f	Ti I (42) 4536.051
53.....	4537.164	0.4	0.001	0.61	20.2f	Unidentified line
54.....	4537.840	0.6	0.001	0.61	20.2f	Unidentified line
55.....	4538.994	0.6	0.001	0.61	20.2f	Fe I (1048) 4538.950
56.....	4539.596	2.4	0.004	0.61	20.2f	Cr II (39) 4539.620
57.....	4540.805	0.6	0.001	0.61	20.2f	Cr I (150) 4540.179
58.....	4541.514	26.0	0.047	0.56	18.5	Fe II (38) 4541.523
59.....	4542.410	1.0	0.002	0.61	20.2f	Fe I (894) 4542.422
60.....	4542.823	0.6	0.001	0.61	20.2f	Cr II (16) 4542.770
61.....	4543.733	0.4	0.001	0.61	20.2f	Cr I (100) 4543.740
62.....	4544.075	2.4	0.004	0.61	20.2f	Ti II (60) 4544.009
63.....	4544.781	1.3	0.002	0.61	20.2f	Ti I (42) 4544.688 Cr II (16) 4544.700

TABLE 1—Continued

<i>N</i>	$\lambda$ (Å)	EW (mÅ)	Depth	FWHM (Å)	$V \sin i$ (km s <sup>-1</sup> )	Identification
64.....	4545.127	3.6	0.006	0.65	21.6	Ti II (30) 4545.144
65.....	4545.480	1.5	0.002	0.61	20.2f	Cr II (16) 4545.490 Fe I (894) 4545.540
66.....	4546.693	0.6	0.001	0.61	20.2f	Fe I (989) 4546.680
67.....	4547.151	1.6	0.003	0.61	20.2f	[Ni I (146) 4547.234]
68.....	4547.852	2.3	0.004	0.61	20.2f	Fe I (755) 4547.851
69.....	4549.240	11.6	0.021	0.56	18.3f	Fe II (186) 4549.214
70.....	4549.473	82.9	0.152	0.56	18.3f	Fe II (38) 4549.467
71.....	4549.635	78.9	0.144	0.56	18.3f	Ti II (82) 4549.622
72.....	4550.718	2.3	0.004	0.61	20.2f	Fe II (KZ) 4550.647
73.....	4552.282	1.7	0.003	0.61	20.2f	Ti II (30) 4552.250
74.....	4552.617	1.2	0.002	0.61	20.2f	[Si III (2) 4552.616]

The weak standard profile is highly unusual. It is clearly flat-bottomed, resulting in a trapezoidal appearance. This is illustrated in Figure 3 which shows features at  $\lambda\lambda 4528-30$  due to Fe I and Ti II. Standard (*dashed*) and purely rotational profiles (*dotted*) have been fitted to these two lines. Note that neither of these fitted profiles is the result of a model atmosphere calculation. The former is a melange of weak line profiles as discussed above, while the latter is simply an analytical relation (cf. Unsöld 1955, eq. [123.11];  $\beta = 0.6$ ). This line pair has been the subject of detailed calculations, discussed below.

We find that the weak features throughout the spectrum show this flat-bottomed shape, so that line blending cannot explain them. Synthesis of sections of the spectrum using the program SYNTHE (Kurucz 1991) has confirmed that line blending is not the origin of the anomalous weak line profiles. Binarity is also an implausible explanation as Reticon spectra taken at different times all show the same line widths (in km s<sup>-1</sup>) for unblended lines of a given strength.

#### 4. OTHER STARS

J. M. F. noted the flat-bottomed profiles of Vega on IIIa-J spectrograms, but not on IIa-O spectrograms. This means that a signal-to-noise ratio of at least order 100 would probably be required to see the phenomenon in other stars. S. J. A. exam-

ined 2.4 Å mm<sup>-1</sup> DAO Reticon spectra, with typical signal-to-noise) ratio of 200, of 42 sharp and moderately sharp-lined ( $v \sin i < 40$  km s<sup>-1</sup>) stars with spectral types between B2 and F7. The spectra of both 10 Tri (HR 675) and  $\nu$  Cap (HR 7773) (Fig. 4) definitely show the weak flat-bottomed lines seen in Vega.

Holweger, Gigas, & Steffen (1986a) and Holweger, Steffen, & Gigas (1986b) presented sections of high-resolution Reticon spectra of sharp-lined B9.5-A2 V stars. Illustrations in these papers suggest that  $\beta$  PsA (HR 8576) and perhaps other spectra, notably  $\nu$  Cap, have flat-bottomed weak lines. The confirmation of the nature of the weak line profiles of  $\nu$  Cap with a different high-resolution spectrograph indicates a non-instrumental origin. The four stars with these profiles have moderate values of  $v \sin i$ ,  $25 \pm 10$  km s<sup>-1</sup> and a spectral type of A1  $\pm$  1.5.

Our examination of the DAO Reticon spectra revealed a few other stars which might have weak lines with profiles intermediate between the flat-bottomed (Vega) and classical rotational types. A number of the early A spectra examined, for example 28 And, 2 Lyn, Sirius, Procyon,  $\beta$  UMa, HR 6775,  $\pi$  Dra, and Deneb, showed no sign of the flat-bottomed profiles for any lines. The contrast between normal and flat-bottomed profiles is illustrated in Figure 5 which shows Vega and Sirius in the

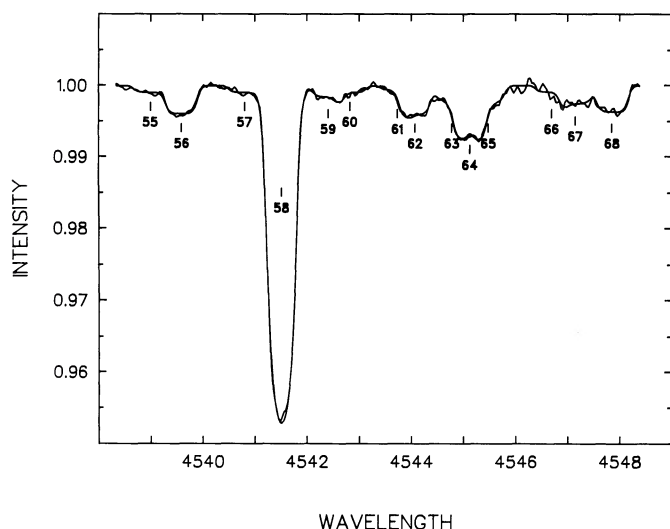


FIG. 2.—The VLINE fit to the spectrum of Vega with spectral line data referenced in Table 1.

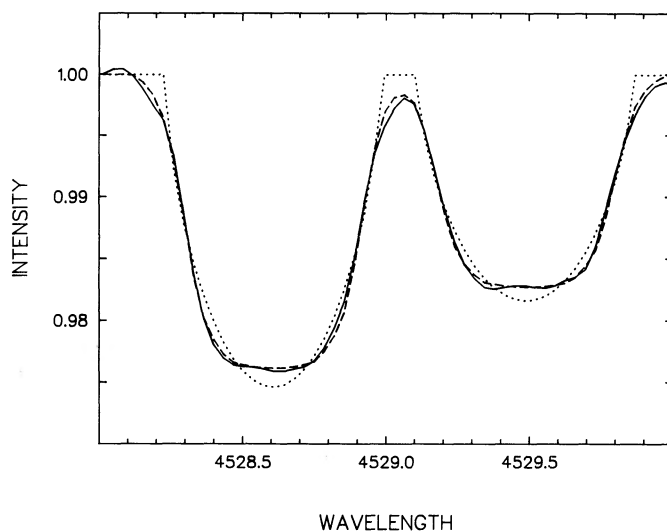


FIG. 3.—The  $\lambda\lambda 4528-30$  features due to Fe I and Ti II. Also shown is the fit of a pure rotational profile with  $\beta = 0.6$  (*dotted line*) and the standard stellar profile (*dashed line*).

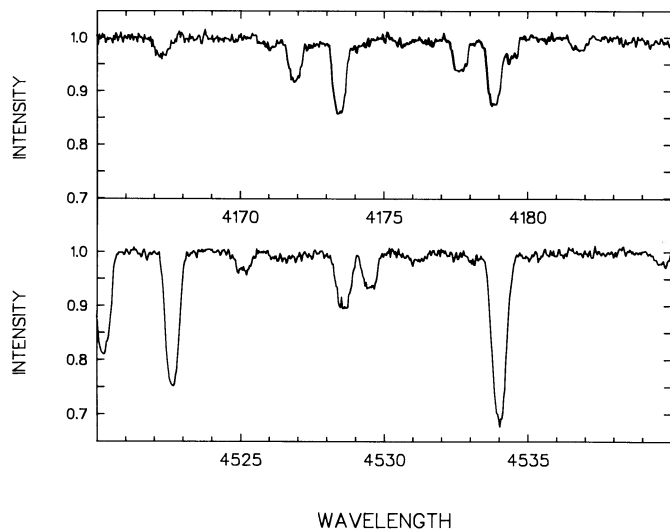


FIG. 4.—The spectra of  $\nu$  Cap ( $\lambda\lambda 4165-85$ ) and 10 Tri ( $\lambda\lambda 4520-40$ ) showing flat-bottomed weak lines.

region  $\lambda\lambda 4735-55$ . The difference in metallicities is also very apparent.

At this time, we do not know how common the flat-bottomed weak line profiles may be. The sharpest lined B, A, and F stars apparently do not show such lines. The known class members simply reflect the programs of the various investigators. Data with signal-to-noise ratio greater than 200 will be required to investigate weak lines in stars with  $v \sin i$  values much greater than about  $40 \text{ km s}^{-1}$ .

### 5. CALCULATIONS

We have attempted to reproduce the observed profiles from model atmosphere calculations. Two basic procedures have been employed in the past. The simplest method is to calculate the profile in the *flux* and convolve the resulting shape with a “rotational profile.” This method requires the detailed calculation of only one line profile. On the other hand, it is not

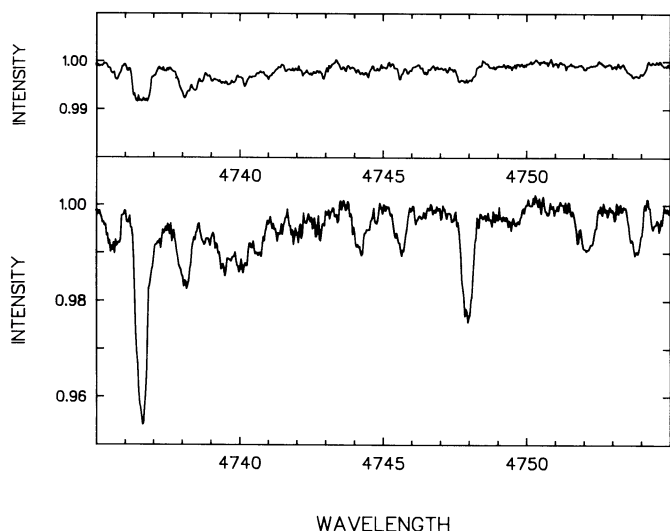


FIG. 5.—The spectra of Vega (*top*) and Sirius ( $\lambda\lambda 4735-55$ ) illustrating the different nature of the line profiles.

rigorous. Gray’s (1976, 1988a) discussions of this *flux method* give useful insight into the procedure and its approximations.

A conceptually correct approach is to calculate the profile for various points on the stellar disk and add the resulting profiles, weighting by the local value of the specific intensity. We shall call this the *intensity method*. It takes explicit account of the variation of the line shape and strength with position on the disk of the star and can be modified to include distortions of the shape of the star and differential rotation (see Collins & Sonnenborn 1977). Slettebak (1985) gives numerous references to this and related techniques.

We have made calculations of weak lines in a model of Vega using both the procedures described above. Neither method can properly account for the observed weak profiles, but we get a better fit with the intensity method.

The intensity and flux methods both make use of intensity at various points on the disk. These may be obtained from model atmosphere calculations or from an assumed limb darkening law. Often, the intensity is represented by a linear expansion in  $\mu$ , or  $\cos \theta$ . Theoretical limb darkening for Vega models is not well described by a linear expansion in  $\cos \theta$ . We made least-squares fits to 20 calculated specific intensities from  $\mu = 0.05$  to  $\mu = 1.0$ , using the form

$$I = 1 + u_1(\mu - 1) + u_2(\mu^2 - 1) + \cdots + u_n(\mu^n - 1).$$

For  $\lambda 4530$ , a linear expansion in  $\mu$  is several percent too faint over most of the disk and becomes nearly 30% too bright at  $\mu = 0.05$ . Four coefficients were needed to keep the errors under 1% in this domain of  $\mu$ .

It is relatively straightforward to modify the flux method to account for a more accurate limb-darkening law. We have made flux calculations using a three-parameter expansion, which reproduces the calculated intensity to better than 1% except at  $\mu = 0.15$  (+1.1% error, too bright) and  $\mu = 0.05$  (−2.5% error). The resulting averaged profiles were indistinguishable, however, from those obtained with a linear fit. It appears that the tendency of the flux method to give too sharp profiles is unrelated to the accuracy of the limb darkening fit.

We have produced intensity-method profiles from two independent programs. First, we used the well-known Kurucz code, whose algorithm for producing rotational profiles is described by Kurucz & Furenlid (1979). C. R. C. made calculations with a program based on the flux code used by Cowley and his coworkers (cf. Cowley & Greenberg 1988) but modified for the specific intensity. It was cast into double precision for use with the weak Vega profiles. A table of profiles was produced for 10 values of  $\mu$ , from 0.05 to 0.95. The rotational profile is made by the addition of profiles interpolated from this table. Two-way quadratic Lagrange interpolation is used to obtain wavelength-shifted profiles for various intermediate values of  $\mu$ . The profiles are weighted by the local values of the specific intensity, which is obtained from a three-parameter fit to the calculated limb-darkening law. The calculations used here employed 900 points distributed uniformly over the stellar disk.

The resulting profile shapes from the Cowley and Kurucz codes are in good agreement and need not be discussed separately. We note that the profiles from the intensity method are flatter on the bottom than those from the flux code. This is presumably because of the increase in the strength of the line from the center to the limb, which adds absorption in the wings of the profile. This effect can be mimicked in a flux calculation by arbitrarily modifying the assumed limb-darkening law.

Unsöld (1955, Fig. 168) and Gray (1976, Fig. 17-5) show the rotational profiles resulting from the flux method both with and without limb darkening. Clearly a flatter profile will result if no limb darkening is assumed. One can, in fact, obtain a very flat profile by assuming a negative value for the coefficient of  $\cos \theta$  in the limb-darkening law, i.e., limb brightening.

We do not think the flat profiles in Vega are likely to be explained by the limb-darkening law. It may be of practical value to note that a flux-method calculation can simulate the shape of an intensity-method profile. This would be accomplished by artificially adjusting the limb-darkening law. This procedure could allow one to save considerable computing time by using the flux-method rather than the intensity-method algorithms. For the present, this suggestion requires more detailed investigation.

### 6. OPTIMUM FITS

We have used the Cowley code to attempt an optimum fit of the pair of lines Fe I  $\lambda 4528.61$  and Ti II  $\lambda 4529.49$ . The results are shown in Figure 6. No macroturbulence is used; the microturbulence is  $1 \text{ km s}^{-1}$ . The stellar profile is broadened by a Gaussian with a FWHM of  $0.074 \text{ \AA}$  to simulate instrumental broadening. The value of  $v \sin i$  found in this "optimum fit" is  $24 \text{ km s}^{-1}$ , slightly larger than in the figures mentioned above.

The fits shown in Figure 6 were obtained from Cowley's ATMOS code described elsewhere. The  $T(\tau)$  is from a Kurucz model for  $T_{\text{eff}} = 9500$ , and  $\log g = 3.5$ . The abundances are those of Adelman & Gulliver (1990), apart from that for helium—here,  $\text{He}/\text{H} = 0.0677$ . Our present purpose is to see if we can account theoretically for the flat-bottomed, weak profiles, and not to establish a definitive abundance or  $v \sin i$ . We shall therefore postpone detailed remarks on these topics to further contributions.

The theoretical fits are impressive. The maximum deviation of the fit to the intensities is less than 0.002 in the range  $\lambda 4528\text{--}30$ . We were able to fit the "quasi" continuum in the range  $\lambda 4527\text{--}28$  with a quadratic relation, yielding a maximum deviation only a factor of 2 smaller: 0.001. Calculations by Adelman & Gulliver show that this region is not completely devoid of line absorption features. Thus, some of the scatter in this region is due to real lines which are not properly accounted for by a quadratic fit. The rms deviations are smaller. We find  $8.4 \times 10^{-4}$  for the  $2 \text{ \AA}$  region containing the line pair and  $4.7 \times 10^{-4}$  for the preceding  $1 \text{ \AA}$  stretch of "quasi" continuum.

If we were to assume that the smaller of these rms deviations (the  $4.7 \times 10^{-4}$ ) were entirely due to noise, the signal-to-noise ratio would be very nearly the reciprocal of this number, some 2100. This is because the "signal" is very nearly the level of the continuum, that is, unity. We have estimated a somewhat higher value, about 3200, using more data.

It is remarkable that we were able to notice the "flatness" of the observed profiles by visual inspection. A plot of the residuals (observed minus calculated) for the region  $\lambda 4528\text{--}30$  is shown in the lower panel of Figure 6. One can see that the observed intensities near the line centers ( $\lambda 4528.5$  and  $4529.5$ ) are larger than the calculations (positive residuals). The residuals become generally negative as the profile first steepens but then become quite small. The residuals become systematic again in the line wings where the observed profiles are too

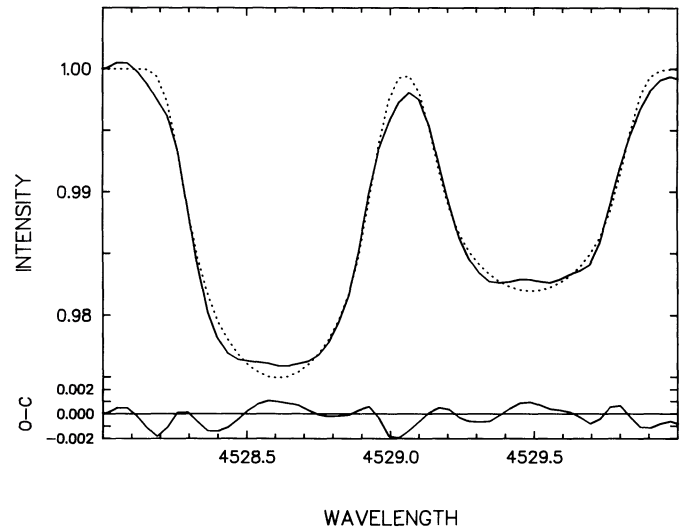


FIG. 6.—An ATMOS model fit (dotted line) for  $T_{\text{e}} = 9500$ ,  $\log g = 3.5$  to the  $\lambda 4528\text{--}30$  features. The lower panel shows the residuals (dashed line), observed — calculated, between the  $\lambda 4528\text{--}30$  features and the model fit.

strong. Extensive tests indicate that these enhanced wings are not the result of the instrumental profile.

### 7. CONCLUSIONS

We are at present unable to account for the small but definite systematic deviations of the Vega profiles from our optimum calculations. We cannot attribute them to instrumental effects. Phenomena intrinsic to the star deserve serious consideration. Rotation, possibly differential rotation, turbulence, and deviations from the plane-parallel model need to be explored.

An intriguing alternative is that the profiles might result from a temperature gradient over the star due to its rotation. If Vega is nearly pole-on, a hypothesis also suggested by Gray (1988b) on the basis of its excess luminosity, then the equatorial regions would have a simulated lower gravity and some atomic lines would be stronger. This might give the same effect as limb brightening, but would depend on the kind of line observed. Since we have concentrated until now on lines of the iron peak elements, the study of lines of other atomic species is important. That no very sharp-lined star has shown Vega-like weak profiles supports a rotational rather than a turbulence explanation. These possibilities need to be investigated as these small, but definite departures from classical line profiles may well contain very important astrophysical information.

We thank James Hesser, Director of the Dominion Astrophysical Observatory, for the observing time; George W. Collins, Richard O. Gray, Graham Hill, Robert L. Kurucz, Arne Slettebak, and Stephenson Yang for useful discussions; and Les Saddlemyer and Doug Bond for help with the observing set-up. We appreciate the encouragement of our colleagues Chris Aikman, Kozo Sadakane, and Masahide Takada-Hidai. Financial support for part of this work was provided to AFG by the National Sciences and Engineering Research Council of Canada and to SJA by NASA grant 5-921 to The Citadel and by grants from The Citadel Development Foundation.

## REFERENCES

- Adelman, S. J., & Gulliver, A. F. 1990, *ApJ*, 348, 712  
Booth, A. J., Blackwell, D. E., & Fletcher, J. M. 1990, *Pub. Dom. Ap. Obs.*, 18, 1  
Cowley, C. R., & Greenberg, M. 1988, *MNRAS*, 232, 763  
Collins, G. W., II, & Sonnenborn, G. H. 1977, *ApJS*, 34, 41  
Gigas, D. 1986, *A&A*, 165, 170  
Gray, D. F. 1976, *The Observation and Analysis of Stellar Photospheres* (New York: Wiley)  
———. 1988a, *Lectures on Spectral-Line Analysis: F, G, and K Stars* (Arva, Ontario: Aylmer Express)  
Gray, R. O. 1988b, *JRASC*, 82, 336  
Gulliver, A. F., & Hill, G. 1990, *PASP*, 102, 1200  
Gulliver, A. F., & Stadel, J. G. 1990, *PASP*, 102, 598  
Hill, G., & Fisher, W. A. 1986, *Pub. Dom. Ap. Obs.*, 16, 159  
Holweger, H., Gigas, D., & Steffen, M. 1986a, *A&A*, 155, 58  
Holweger, H., Steffen, M., & Gigas, D. 1986b, *A&A*, 163, 333  
Kurucz, R. L. 1991, in preparation.  
Kurucz, R. L., & Furenlid, I. 1979, *Sample Spectral Atlas of Sirius* (SAO Special Report 387)  
Sadakane, K., Nishimura, M., & Hirata, R. 1986, *PASJ*, 215  
Slettebak, A. E. 1985, in *IAU Symposium 111, Calibration of Fundamental Stellar Quantities*, ed. D. S. Hayes, L. E. Pasinetti, & A. G. D. Philip (Dordrecht: Reidel), 163  
Unsöld, A. 1955, *Physik der Sternatmosphären* (2d ed.; Berlin: Springer)  
Walker, G. A. H., Johnson, R., Richardson, D., Campbell, B., Irwin, A. W., & Yang, S. 1990, *PASP*, 102, 1418